# Towards a New Understanding of the Low-energy Excitations in the Even-even Nuclei

H. Mach, B. Fogelberg, M. Hellström, D. Jerrestam, and L. Spanier
*Department of Neutron Research, University of Uppsala, S-61182 Nyköping, Sweden*

**Abstract:** The nuclear structure studies of the neutron-rich nuclei represent a vibrant and fast progressing field. A review is given of a few regions of critical importance to nuclear structure that are now accessible exclusively by mass separation techniques of fission or spallation products. In particular, recent results on the doubly-magic $^{132}$Sn are discussed as well as those for the low-lying bands in the neutron-rich A$\sim$100 and A$\sim$150 regions: discrepancies between the shape-coexistence interpretation and the experimental results on the shape-coexistence regions of heavy Sr/Zr, Cd/Sn and Sm/Gd, the 'correspondence interpretation' of transitional Sm/Gd, suggestion that the $\beta'$ band in the transitional Sm/Gd nuclei represents a new mode of intrinsic excitation in par with the $\beta$ and $\gamma$ modes, and the issue of 'di-nature' of the excited $0^+$ bands. The latter, relates to a seemingly contradictory feature shown by the excited $0^+$ bands, which behave like a weakly mixed (independent) second ground state with its individual properties (like moment of inertia) and at the same time like proper members of the g.s. structure.

## Preface

The title of this talk is meant to be provocative. After all, the presently used nuclear models provide quite adequate description of many nuclear phenomena, and yet we know that these models are not the ultimate theory. There is a growing list of results that are poorly explained, although some model refinements (like expansion of the model space or inclusion of additional terms) could account for those discrepancies. On the other hand, there are also results that seem to contradict the model assumptions outright and challenge our intuitive understanding of the nuclear structure. As such results have a unique capacity to unravel new phenomena and lead towards the next generation of theoretical models, it is these results (or rather a selection of them) that are discussed here. Included is also a brief presentation of our most recent experimental results on the neutron-rich nuclei obtained at the fission-product mass separator OSIRIS at Studsvik. The reader is referred, however, to the original publications for a complete discussion.

## 1. Introduction

The fission-product mass separator OSIRIS provides intense beams of several hundred neutron-rich nuclei making it possible to study their structure in some de-

tail. Among these nuclei, now accessible exclusively via mass separation techniques of fission or spallation products, there are a few regions that are of critical interest to nuclear spectroscopy.

Our current activities at OSIRIS have been focussed on improvements of the ion–source performance and separation techniques [1,2] and on the implementation of a $\beta\gamma\gamma(t)$ fast timing method [3,4] that proved itself so powerful in the domain of the neutron–rich nuclei. These developments allow not only to access the more exotic nuclei (like the neutron–rich A$\sim$150 region) but also to study them in more detail including the measurement of transition rates. Our recent experiments have been focussed on the doubly magic $^{132}$Sn and on the band structures in the heavy Nd–Sm nuclei.

The nuclei at doubly closed shells, like $^{132}$Sn, reveal the basic nuclear properties — level energies of single–particle states and specific single–particle matrix elements. Furthermore, they provide information on deep polarization effects and on the meson exchange currents in the multi–nucleon systems. For the medium heavy nuclei (A>50) only the structure of doubly magic $^{208}$Pb has been probed by a variety of experimental techniques [5] yielding crucial model parameters for the interaction of nucleons. As for the other cases, neither $^{78}$Ni nor $^{100}$Sn have been observed experimentally, while $^{132}$Sn has been relatively poorly known, although it has been observed [6] in the $\beta^-$ decay of $^{132}$In. The severe lack of information is caused by the difficulty in accessing these nuclei placed far–off stability line.

Recently, Fogelberg *et al.* [7] have reported the first results from a detailed study of $^{132}$Sn using $\gamma\gamma(\theta)$ and fast–timing $\beta\gamma\gamma(t)$ delayed coincidence spectroscopy performed at the improved OSIRIS ISOL–facility at Studsvik. As a result of this work, discussed in Section 3, the number of known excited states of $^{132}$Sn has been more than doubled yielding states of five different particle–hole multiplets. Four level half–lives in the sub–nanosecond range have been determined, from which transition probabilities of 12 intra– and inter–multiplet $\gamma$ rays have been deduced.

The heavy Nd–Sm isotopes represent the other class of nuclei — those placed away from closed shells and characterized by the little understood interplay between quadrupole and octupole excitation modes and quasiparticle excitations. The heavy Nd–Sm nuclei are located in a doubly transitional region: from spherical to quadrupole deformed shapes at N=88/90 [8], and from octupole vibrational near $^{146}$Gd [9] to octupole deformed (or soft towards deformation) near $^{146}$Ba [10]. We have investigated $^{152}$Nd [11,12] and $^{152,156}$Sm [13,14] as discussed in Sections 4 and 5. In particular, the new results reveal an unexpectedly strong influence of selected quasiparticle configurations on the structure of the low–lying bands at the energies about half the pairing gap ($E_x\sim$700 keV).

In $^{152}$Sm, we have measured [13] the lifetimes and $\gamma$ branching ratios for the $0_3^+$ and $0_4^+$ states. The B(E2) and $\rho^2$(E0) rates for the $0_3^+$ band (long interpreted [8] as a classical case of the shape–coexisting 'spherical' band) were found to be well reproduced by the pairing–plus–quadrupole (PPQ) calculations [15] which show no

shape–coexisting minima. Furthermore, we interpret the energy and transition rate systematics for the Sm–Gd nuclei as supporting the correspondence relations [16,17] between levels of the quadrupole vibrational multiplets in the spherical nuclei and the ground state (g.s.), $\beta$, and $\gamma$ bands in the deformed nuclei extended to include the $0_3^+$ ($\beta'$) states as suggested by Sakai [17]. No distinction is made for the shape–coexisting intruder states. Moreover, a number of features suggest that the $\beta'$ band likely represents a new mode of intrinsic excitation in par with the $\beta$ and $\gamma$ modes. These results are discussed in Section 6.

In Section 7 we elaborate on the issue of 'di–nature' of the excited $0^+$ bands [18], which generally show a seemingly contradictory feature, i.e. the 'shape–coexisting' bands which moments of inertia vastly differ from that of the ground state band, often display fast B(E2) rates towards (and also weak mixing with) the lower–lying levels of the g.s. structure.

However, as a starting point to this Lecture we take the A$\sim$100 region where the most abrupt transition from spherical to deformed shapes takes place. This unique and yet largely unknown region has already shown a wealth of surprising results. Some of our recent findings (by the TRISTAN/BNL, JOSEF/Jülich and OSIRIS/Studsvik collaborations) have been discussed at the previous Zakopane School [19] and are briefly highlighted below.

## 2. A$\sim$100

The most interesting phenomena in the A$\sim$100 region seem to be concentrated along the heavy Sr and Zr nuclei as they undergo a spectacular transition from spherical to quadrupole defomed shapes by an addition of a mere neutron pair. With our recent lifetime measurements of the $2_1^+$ states in $^{90-98}$Sr [20–22] the systematics of the intrinsic quadrupole moments $Q_o$ became complete for the whole chain of even–even Sr nuclei, and thus it was possible to demonstrate [22] for the first time the abruptness of this transition as seen in Fig. 1. This abruptness is related to the existence of two flat regions for the spherical and deformed shapes. In Fig. 1 the dashed lines at $Q_o^{av}$=0.96 b for N=50–58 and at $Q_o^{av}$=3.79 b for N=59–62 represent the average values for those groups of nuclei. The abrupt transition from spherical to deformed shape is clearly visible at N=59.

The newly measured B(E2; $2_1^+ \rightarrow 0_1^+$) rates provide additional evidence for a close similarity between Sr and Zr nuclei and a strong argument for their exceptional sphericity as $^{88-96}$Sr and $^{90-98}$Zr show the lowest B(E2) values known for nuclei with A>56, second only to $^{204-210}$Pb [22]. Until recently, it was the sudden appearence of a strong deformation at N=60 that was considered particularly puzzling [23,24]. However, as can be seen in Fig. 1, the quadrupole moment for N=60 hardly appears exceptional, but rather close to the value that would be attained anyhow if a gradual progress of deformation took place instead. It is thus the spherical nuclei, and not the deformed ones, that exhibit exceptional B(E2) strengths and merit a close theoretical investigation.

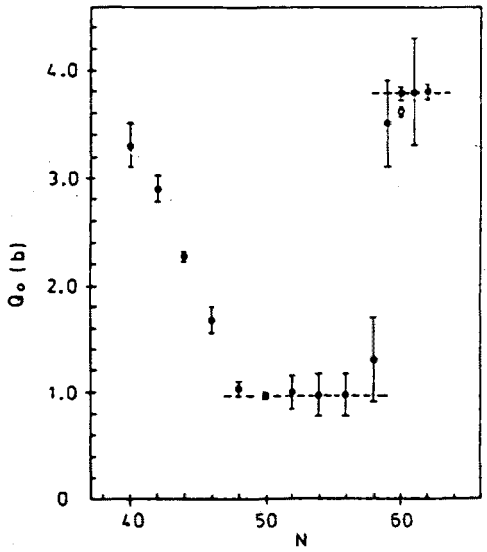


**Figure 1** Intrinsic quadrupole moments $Q_o$ (deduced from the B(E2) values) as a function of neutron number, N, for Sr nuclei (from Ref. [22]).

Yet very few theoretical studies have been performed for A~100. The challenge of this region seems beyond the capabilities of most models, unable neither to deal with such exceptionally sharp discontinuities in nuclear properties nor to treat, on equal footing, the extreme limits of nuclear structure: doubly closed subshells effects and strong deformation. These features are not only displayed by the neighbouring nuclei but also as 'shape–coexistence' within the individual structures.

In the 'shape–coexistence' picture two structures, spherical and deformed, coexist in a nucleus.† In the N≤58 nuclei the g.s. structure is spherical while the excited one is deformed. The latter lowers down in the excitation energy with the increased neutron number and becomes the g.s. at N=60. Although various theoretical models [23,24,26] predict strong mixing between the spherical and deformed configurations, only a weak mixing is evident from the most recent data on the N=56 [27] and N=60 [21,28] nuclei. These conclusions, however, are also model dependent, based largely on the interpretation of the exceptionally strong E0 rates that proliferate in this region.

The identification of the $0^+$ states — the band–heads of the deformed excited

† The term *shape–coexistence*, which has been derived phenomenologically and implies distinctive features for the shape–coexisting bands, is not justified for the present models where strong mixing dilutes the identities of levels (see also comments in Ref. [25]). Nevertheless, we label that way models specifically derived for the shape–coexisting nuclei.

bands — is particularly confusing in the crucial N=58 Sr and Zr nuclei where various claims and counter–claims have been made [29–32]. (The lack of data on these nuclei is surprising since the corresponding beams are easily produced at the fission–product mass separators.) However, the new data on $^{96}$Sr has unravelled [19,33] almost mirror correspondence between $^{96}$Sr and a series of $^{116,118,120}$Sn nuclei (see Fig. 2) based on a similar sequence of the lowest–lying levels, their relative excitation energies, and the E2 and E0 transition rates. This correspondence raises three issues:

(i) it points towards the $0_2^+$ state being the deformed 'shape–coexisting' state in $^{96}$Sr,

(ii) it gives further evidence for the exceptional sphericity of the g.s. structure in $^{96}$Sr (since a comparison is made to the N=50 nuclei), and

(iii) it undermines the theoretical result [25] that the close–lying $0_2^+$ and $0_3^+$ states 'interchange their transition rates' via a strong and peculiar mixing or, to say it differently, via a constuctive/destructive interference of the vibrational and rotational configurations.

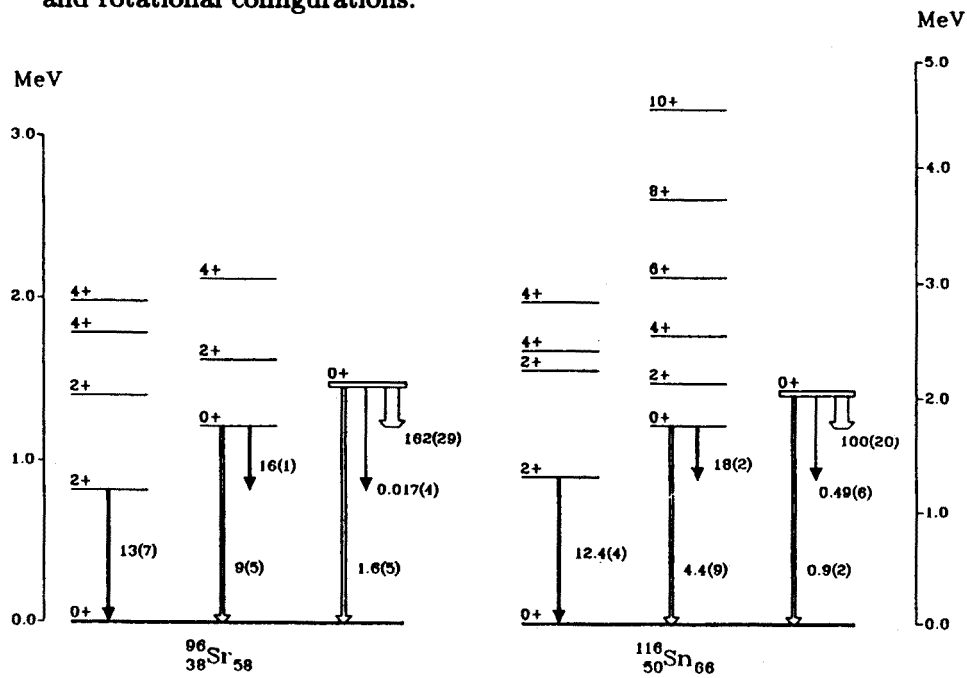


**Figure 2** The mirror correspondence between the lowest–lying levels in $^{96}$Sr and $^{116}$Sn. The E2 transitions are marked by solid arrows with the B(E2) rates in W.u. Similarly E0 transitions are marked by open arrows with the $\rho^2$(E0) rates in $\times 10^3$ units (from Ref. [33]).

Point (iii) requires some explanation. In the shape–coexisting model [25] the de-

formed $0^+$ band–head has an intruder configuration, and thus would decay to the vibrational $2_1^+$ state via a strongly hindered isomeric transition as compared to a fast transition from the second–phonon $0^+$ state. Experimentally (consider $^{116}$Sn in Fig. 2) one observes the opposite; the 'intruder' state decays via a fast transition with B(E2; $0_2^+ \rightarrow 2_1^+$)=18 W.u. while a close–lying $0_3^+$ state decays via a slow B(E2; $0_3^+ \rightarrow 2_1^+$) rate of 0.5 W.u. Note a fast E0 $0_3^+ \rightarrow 0_2^+$ transition that is frequently taken as evidence [26] for a strong mixing of these $0^+$ states. Indeed the 'shape–coexisting model' calculations reproduce [25] the aforementioned transition rates provided that the $0_3^+$ state is the $0^+$ state of the second phonon multiplet and that the $0_2^+$ and $0_3^+$ states are strongly mixed. However, the constructive/destructive interference of the vibrational and rotational configurations, leading to the required 'interchange of transition rates' for the excited $0^+$ states, occurs only for a specific mixing. The argument against such a scenario raised in (iii) is that an occurence of such specific mixing depends on a unique combination of a few factors — a rare condition to be fulfilled for one nucleus let alone for a group of (Sr, Sn and Cd and other) nuclei (see also Ref. [34]).

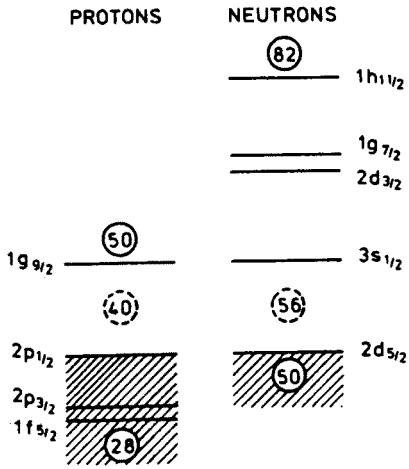


**Figure 3** Schematic representation of subshell orbits at $^{96}$Zr (from Ref. [40]).

The correspondence of $^{96}$Sr to $^{116-120}$Sn provides an interesting link to the well–known Cd/Sn region, and yet it only adds to the 'puzzle of the $0^+$ states' as the recent experimental studies in the Cd/Sn region challenge the shape–coexistence model [34,38,39]. An almost complete set of reduced E2 matrix elements measured for the lowest–lying states in $^{114}$Cd was found [34] to be in better agreement with predictions by the harmonic vibrator model than by various shape–coexistence models. (In particular, the $0_2^+$ and $0_3^+$ states, see Fig. 2, can be simply interpretated as the 2–phonon and 3–phonon vibrational states.) The most basic tenet of the shape–coexisting model for the Cd nuclei is the V–shape lowering and raising

of the intruder configuration near the mid–shell region [35,36] — leading to the model predictions [36] (see also the shape–coexistence model calculations by Heyde and Van Isacker for $^{118,120}$Cd quoted in Ref. [37]) that are contradicted by the experimental results [38,39]. Another tenet of the model calculations is the strong mixing of the close–lying states [25,35,36] (which neccessitates these levels to loose their identity and to be strongly displaced from their unperturbed positions) is also contradicted by the experimental evidence [34,39]. As discussed above, there is no evidence [21,27,28] for a strong mixing of the shape–coexisting states in the A∼100 region as well. Clearly, the issue of 'shape–coexistence' must be addressed anew as the currently used 'shape–coexistence' models are found inadequate. This issue will be discussed again in Sections 5–7.

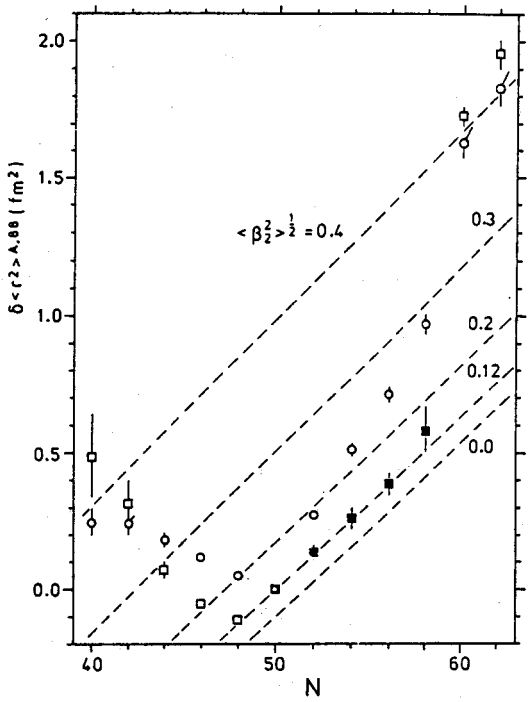


**Figure 4** Comparison of measured (dots) and calculated (squares) changes in mean–square charge radii for $^{78-100}$Sr with respect to $^{88}$Sr (from Ref. [22]).

The unusual features of the A∼100 region result from a competition between low– (e.g.: $\nu s_{1/2}$) and high–spin (e.g.: $\nu h_{11/2}$) orbits near the Fermi level, see Fig. 3. The effect of strong subshell closures culminates in $^{96}$Zr, which represents a unique case of a doubly closed subshell nucleus quite removed from major shell closures. In line with this claim, the lowest energy excitations in $^{96}$Zr are of the particle–hole type [40]. There are two unusual features in this nucleus that are characteristic of

nuclei in the doubly magic regions: a fast first forbidden $^{96}Y^g$ $0^- \rightarrow 0^+$ $^{96}Zr^g$ $\beta^-$ transition with $\log ft = 5.6$ [41] and a fast B(E3; $3_1^- \rightarrow 0_1^+$) rate of ~70 W.u. [42,43] (the fastest known).

The exceptional strength of the B(E3) transition in $^{96}$Zr has not been fully explained [43], although it points towards unexpected softness towards octupole deformation right at the point of the shape transition. The interplay of the quadrupole and octupole excitation modes in the heavy Sr and Zr nuclei has not been fully explored neither from the theoretical nor from the experimental points of view. Yet the observed discrepancy between the mean-square charge radii $\delta < r^2 >$ measured for the $^{78-100}$Sr nuclei by laser spectroscopy techniques [44] and the values calculated from the B(E2) rates (see Fig. 4) can be largely accounted for by the enhanced octupole collectivity [22]. The issue, however, remains open and subject to vigorous theoretical investigations as it is not completely certain whether in this comparison we measure and calculate the same quantity. To summarize:

- the exceptional 'spherical' or 'doubly-magic' features observed in the A~100 region require further detailed shell-model calculations with a better mapping of the fermion interactions obtained (ideally) from the doubly-magic nuclei close to this region, i.e.: $^{78}$Ni and $^{100,132}$Sn;
- the discrepancies related to the presently used shape-coexistence models must be systematized and resolved in order to lead towards the microscopic-macroscopic models that may satisfactorily handle shape-coexistence in such extreme forms.

These issues are discussed further in the following sections.

## 3. Detailed Spectroscopy of $^{132}$Sn

Fogelberg *et al.* [7] have reported the first results from a detailed study of $^{132}$Sn populated in a $\beta^-$ decay of $^{132}$In. Results from the $\gamma\gamma(\theta)$ and fast timing $\beta\gamma\gamma$(t) coincidences are summarized in Fig. 5 and Table 1. One should note, that the data of Fig. 5 is of preliminary nature as the analysis of the $\gamma\gamma(\theta)$ coincidence data is still in progress. The present sub-division of levels need not be correct in all cases. Similarly, the order of the 1823.1- and the 1035.8-keV transitions is not firmly established. Furthermore, the lifetime measurement, although fully analysed, represents a preliminary effort designed to identify the optimal conditions for a full run (with much improved electronics and statistics) to be performed at a later time this year. The present results are nevertheless impressive. It is estimated that less than five percent of the $\beta$-transition intensity of $^{132}$In feeding bound states of $^{132}$Sn is missing from the scheme.

### 3.1 Positive parity states

The previously suggested [45] $7^+$ state at 4918.5 keV has now been firmly established, while a new $5^+$ level at 4885.3 keV has been tentatively assigned. All

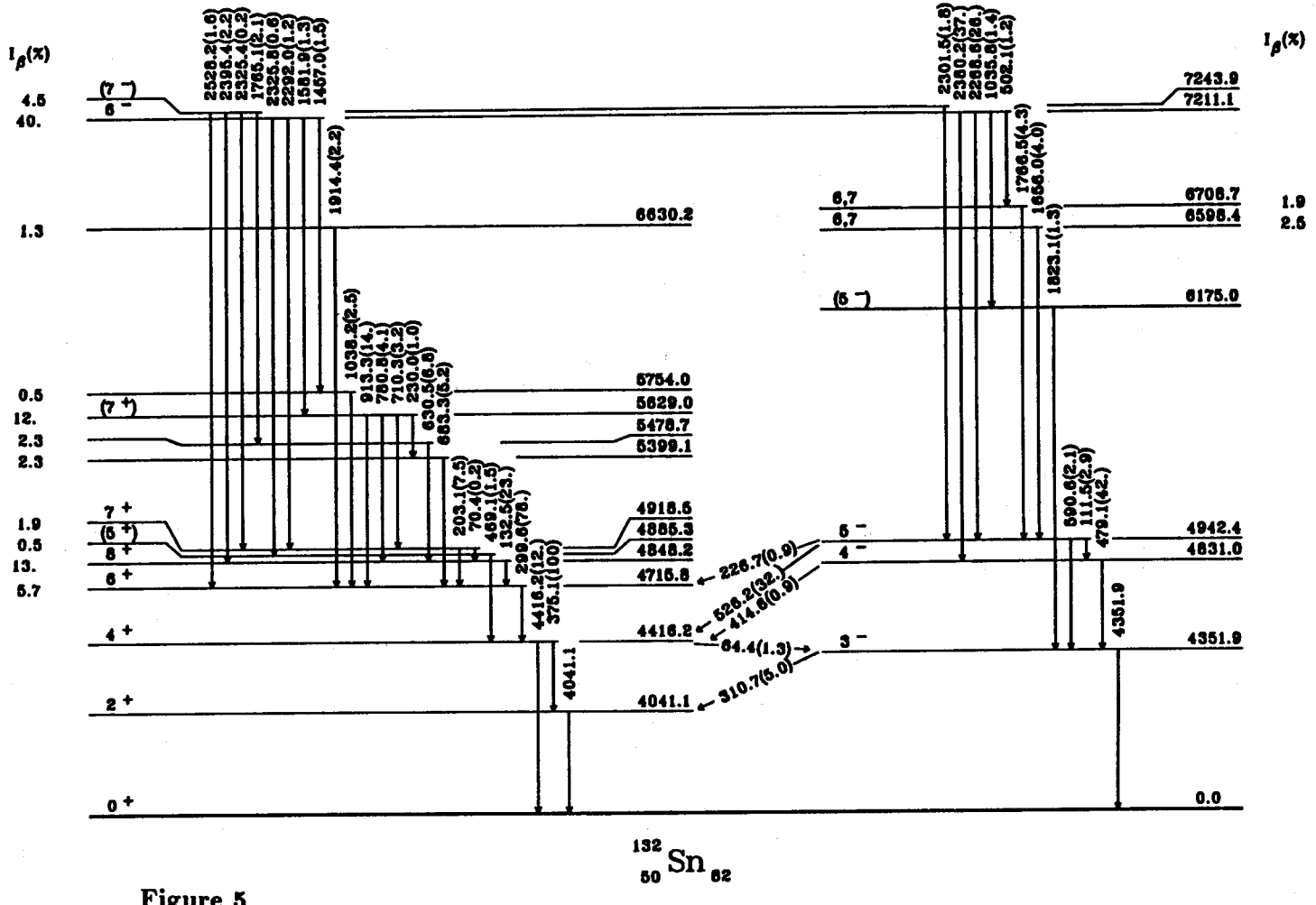
$I_\beta$(%)
4.5
40.
1.3
0.5
12.
2.3
2.3
1.9
0.5
13.
5.7
2528.2(1.6)
2395.4(2.2)
2325.4(0.2)
1765.1(2.1)
2325.8(0.6)
2292.0(1.2)
1581.9(1.3)
1457.0(1.5)
1914.4(2.2)
1038.2(2.5)
913.3(14.)
780.8(4.1)
710.3(3.2)
630.5(6.6)
583.3(5.2)
203.1(7.5)
70.4(0.2)
469.1(1.5)
132.5(23.)
299.8(78.)
4416.2(12.)
375.1(100)
4041.1
6630.2
5754.0
5629.0
5478.7
5399.1
4918.5
4885.3
4848.2
4715.8
4416.2
4041.1
0.0
226.7(0.9)
526.2(32.)
414.8(0.9)
64.4(1.3)
310.7(5.0)
2301.5(1.6)
2380.2(37.)
2268.5(26.)
1035.8(1.4)
502.1(1.2)
1766.5(4.3)
1656.0(4.0)
1823.1(1.3)
590.6(2.1)
111.5(2.9)
479.1(42.)
4351.9
7243.9
7211.1
6708.7
6598.4
6175.0
4942.4
4831.0
4351.9
0.0
1.9
2.6
$^{132}_{50}Sn_{82}$

**Figure 5**

**Table 1** Half-lives in $^{132}$Sn and $^{132}$Sb measured at OSIRIS (from Ref. [7]).

| Nucleus | Level (keV) | $T_{1/2}$ OSIRIS [7] | $T_{1/2}$ (Previous work [6]) |
|---|---|---|---|
| $^{132}$Sn | 4416 | 3.9(4) ns [a] | 4.0(3) 5.6(4) 2.1(3) ns |
| | 4716 | 21.8(35) ns [a] | 21.5(5) 20.2(8) ns |
| | 4831 | 26(10) ps | |
| | 4848 | | 1.98(5) $\mu$s |
| | 4919 | 39(21) ps | <0.5 ns |
| | 4942 | 39(18) ps | |
| | 5399 | $\leq$40 ps | |
| | 5479 | $\leq$30 ps | |
| | 5629 | 29(15) ps | |
| $^{132}$Sb | 86 | 14.9(5) ns [a] | 14.8(18) ns |
| | 426 | 23(8) ps | $\leq$2 ns |
| | 1078 | $\leq$13 ps | $\leq$2 ns |
| | 1325 | $\leq$50 ps | $\leq$0.8 ns |

[a] Value deduced from slope fitting in the $\beta\gamma\gamma$(t) experiment.

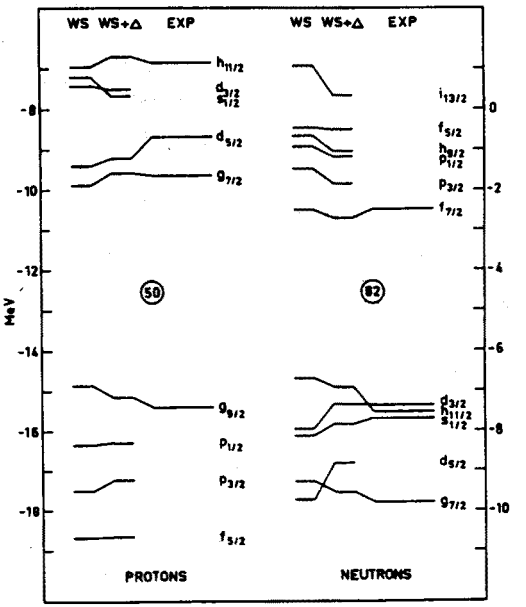


**Figure 6** Schematic representation of subshell orbits at $^{132}$Sn (from [45]).

**Table 2** B($\lambda$) transition rates deduced for $^{132}$Sn in Ref. [7].

| Level (keV) | $J^\pi$ | $T_{1/2}$ | $\gamma$ out | $I_\gamma$ | Mult. | $F_W$ [a] | B($\lambda$) [a,b] |
|---|---|---|---|---|---|---|---|
| 4416 | $4^+$ | 3.9(4) ns | 64.4 | 1.3 | E1 | 3.6+5 | 4.6−8 |
| | | | 375.1 | 100 | E2 | 2.5 | 1.7−3 |
| | | | 4416.2 | 12 | E4 | 0.17 | |
| 4716 | $6^+$ | 21.5(5) ns | 299.6 | 78 | E2 | 3.9 | 1.05−3 |
| 4848 | $8^+$ | 1.98(5) $\mu$s | 132.5 | 23 | E2 | 9.3 | 4.35−4 |
| 4831 | $4^-$ | 26(10) ps | 414.6 | 0.9 | E1 | 3.4+5 | 4.9−8 |
| | | | 479.1 | 42 | M1 | 131 | 1.4−2 |
| 4919 | $7^+$ | 39(21) ps | 70.4 | 0.20 | M1 | 27 | 6.7−2 |
| | | | 203.1 | 7.5 | M1 | 17 | 10.6−2 |
| 4942 | $5^-$ | 39(18) ps | 111.5 | 2.9 | M1 | 33 | 5.5−2 |
| | | | 226.7 | 0.9 | E1 | 7.6+4 | 2.2−7 |
| | | | 526.2 | 32 | E1 | 2.7+4 | 6.2−7 |
| | | | 590.6 | 2.1 | E2 | 3.7 | 1.1−3 |
| 5629 | $7^+$ | 29(15) ps | 230.0 | 1.0 | M1 | 357 | 5.1−3 |
| | | | 710.3 | 3.2 | M1 | 3.3+3 | 5.5−4 |
| | | | 780.8 | 4.1 | M1 | 3.4+3 | 5.3−4 |
| | | | 913.3 | 14 | M1 | 1.6+3 | 11.3−4 |

[a] Units used E1 [$e^2b$], M1 [$\mu_N^2$], and E2 [$e^2b^2$].
[b] Notation: 5.1+5 means $5.1\times10^5$, 3.3−8 means $3.3\times10^{-8}$.

positive parity states below 5 MeV likely belong to the $\nu f_{7/2}\nu h_{11/2}^{-1}$ multiplet (see Fig. 6 for the configuration of orbits). This assumption is supported by the fast M1 transition rates from the $7^+$ level that confirm the common microscopic structure of the levels involved. For the 70.4 and 203.1 keV transitions, which can be taken to be predominantly of M1 multipolarity, the B(M1) rates deduced from the level half-life (see Table 2) are of the order of 0.04 W.u., thus typical of the M1 transitions within a particle–hole multiplet.

The four levels at ~6 MeV most likely have positive parity and are members of the $\pi g_{7/2}\pi g_{9/2}^{-1}$ multiplet. The excitation energy and the observed $\beta^-$ feeding of the most strongly populated state at 5629.0 keV agree with the predictions [45] for the $7^+$ member of the multiplet. From its half-life, and again assuming a M1 multipolarity of the depopulating transitions, one finds hindrance factors well in excess of $10^3$ for the transitions to the previously discussed $\nu\nu^{-1}$ levels below 5 MeV. As expected these transitions are strongly hindered as a consequence of the

configurations involved. In contrast, the 230.0–keV transition from the same level is substantially less hindered, suggesting it connects two levels of the $\pi\pi^{-1}$ multiplet.

### 3.2 Negative parity states

For the negative parity states three new transitions have been observed and the lifetimes have been measured for the $4^-$ and $5^-$ levels of the $\nu f_{7/2}\nu d_{3/2}^{-1}$ multiplet. As seen in Table 2, a strong hindrance is observed for the E1 transitions to the positive parity states, as such transitions are strongly forbidden in the case of pure configurations. The 111.5– and 479.1–keV transitions (assumed to be M1) show the low hindrance expected for intra–multiplet M1 transitions. The 590.6–keV cross–over transition can only be of E2 multipolarity. Its B(E2) rate of $\sim 10^{-3}\ e^2b^2$ is very similar to those observed [46] between the even–spin states of the lowest–lying positive parity multiplet, see Table 2.

### 3.3 Higher–lying levels

In the decay of $^{132}$In, the most intense $\beta$ transition populates a level at 7211.1 keV for which $J^\pi=6^-$ and configuration $\nu f_{7/2}\nu g_{7/2}^{-1}$ have been firmly assigned [45]. This $\beta$ transition and the main $\gamma$–ray decay of the 7211.1–keV level are equivalent to the $\beta$–decay of $^{131}$In and the subsequent $\gamma$–ray decay of the $\nu g_{7/2}^{-1}$ state in $^{131}$Sn [47]. In $^{132}$Sn the $\beta^-$ feeding to the $7^-$ state in the same multiplet is predicted [45] to be 1/8 of the feeding to the 7211.1–keV level. As the level at 7243.9 keV follows this prediction, it is adopted as the $7^-$ member of the $\nu f_{7/2}\nu g_{7/2}^{-1}$ multiplet.

### 3.4 Further Studies in the $^{132}$Sn and $^{78}$Ni regions

The new results confirm the ability to study $^{132}$Sn, and by default a few other nuclei in this crucial region, in great detail at the improved OSIRIS ISOL–facility at Studsvik. Furthermore, it also improves the chances to study nuclei in the immediate vicinity of doubly–magic $^{78}$Ni.

The $\gamma\gamma(\theta)$ setup used for $^{132}$Sn involved five ordinary Ge and six BGO detectors. The sensitivity of such measurements on $^{132}$Sn (and other rare species) can be much improved with a large detector array with Compton suppressed Ge detectors. Even the use of an 'old generation' (e.g., TESSA) array over a limited period of time at OSIRIS could significanlty improve the identification of rare decays, weakly populated levels or weak, but crucial, decay branchings. Such possibilities should certainly be explored, leading perhaps to data much enriched over those described here, although even these first results represent an extraordinary improvement over the previous knowledge of $^{132}$Sn.

## 4. Band Structure in $^{152}$Nd

Nuclei in the heavy Ba–Sm region feature the lowest–lying $1_1^-$ states in the rare–earth region [48,49] with the $K^\pi=0^-$ excitations well below 800 keV in $^{148}$Ce

and $^{144-148}$Ba. The properties of these states show strong fluctuations. The B(E1) branching ratios and the B(E1) rates show abrupt changes in $^{146}$Ba [10], while sudden increase in excitation energy is observed for the $K^\pi=0^-$ band in $^{152}$Nd [49,50].

Although this region is subject to many theoretical studies exploring the crucial interplay of quadrupole and octupole modes of excitation, any critical model testing is handicapped by the scarcity of data on the negative parity states. It is thus indeed fortunate that the odd–odd nuclei in the A=140–160 region often have negative–parity ground states which, via the $\beta^-$ decay, preferentially populate states with negative parity in their daughter even–even nuclei. This provides efficient means, and in fact a unique opportunity, to study the systematics of the negative–parity states of different types (including the octupole bands) in this region. Until recently, however, this region has been inaccessible to direct spectroscopic studies. The improvements of the target and ion source at OSIRIS [1,2] and other facilities (e.g.: Ref. [51]) have made it possible to overcome this problem.

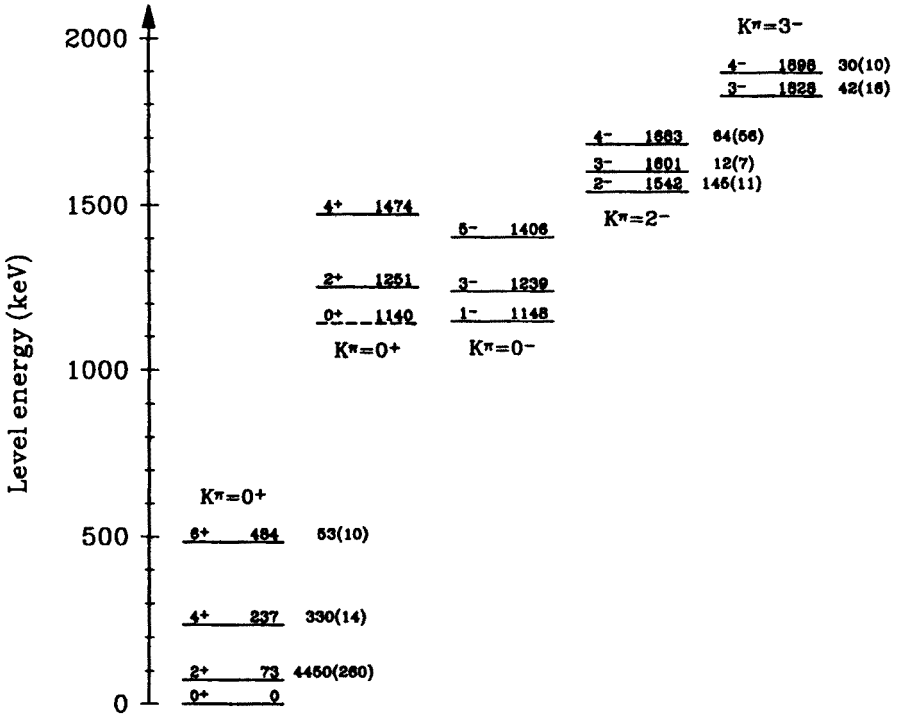


**Figure 7** Ground state and $K^\pi=0^+$, $0^-$, $2^-$, and $3^-$ bands identified in $^{152}$Nd. The new half–lives (in ps) are listed to the right of the level bar (from Ref. [12]).

Recently, Hellström *et al.* reported [11,12,52] on the detailed $\gamma$–ray spectroscopy of levels in $^{152}$Nd populated in the $\beta^-$ decay of $^{152}$Pr. The measurements

included $\gamma\gamma(\theta)$ and fast timing $\beta\gamma\gamma(t)$ coincidences. The results for the negative and positive parity states are discussed below.

### 4.1 Negative parity bands

The results for the negative parity bands are summarized in Fig. 7. Bands with $K^\pi=0^-$, $2^-$, and $3^-$ have been firmly identified, while new half-lives have been measured for 8 levels as indicated in the figure. There is no evidence for levels of a $K^\pi=1^-$ band. The new results for $^{152}$Nd and $^{156}$Sm [14] are combined into a new systematics of the octupole bands.

**Figure 8** (below left) Excitation energies of the $K^\pi=0^-$ bands in the A=150 region. Data for a given element are connected by a solid line (from Ref. [12]).

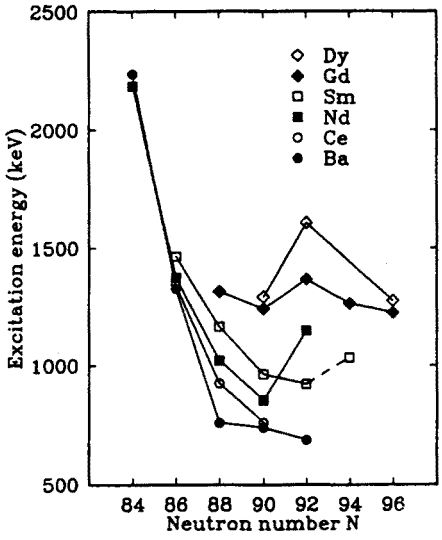


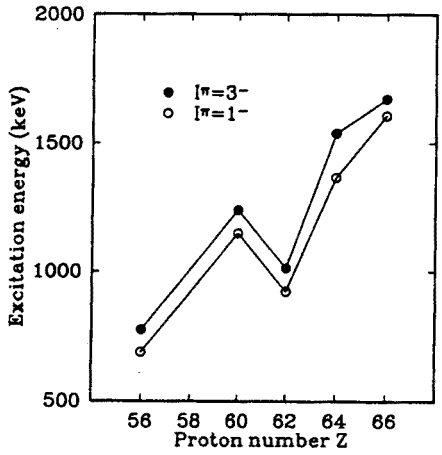


**Figure 9** (above right) Excitation energies of the $I^\pi=1^-$ and $3^-$ members of the $K^\pi=0^-$ bands at N=92. Note that in this figure it is the Sm points (Z=62) and not the Nd ones (Z=60) that appear to be abruptly displaced from the otherwise smooth systematics. (from Ref. [12]).

The $K^\pi=0^-$ systematics of Fig. 8 shows a rather smooth and gradual decrease of the excitation energies with both increasing neutron and decreasing proton numbers towards a minimum near $^{146-148}$Ba (N=90–92). A singular departure from the smooth systematics appears at $^{152}$Nd (N=92) where a sharp jump by ~300 keV is noticed. However, in the N=92 systematics plotted in Fig. 9, it is the Sm points (Z=62) and not the Nd points (Z=60) that shows a sudden jump. This confusing pattern may become clear as new data become available.

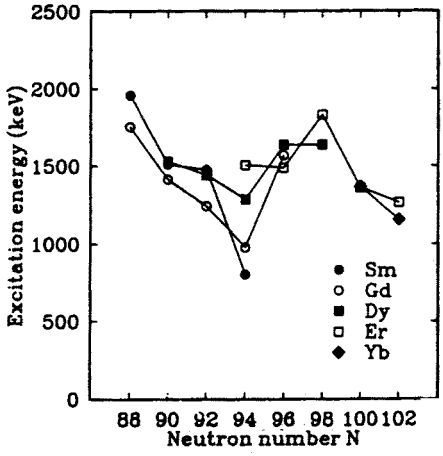


**Figure 10** Excitation energies of the $K^{\pi}=1^{-}$ bands in the A=150 region. Data for a given element are connected by a solid line. (from Ref. [12]).

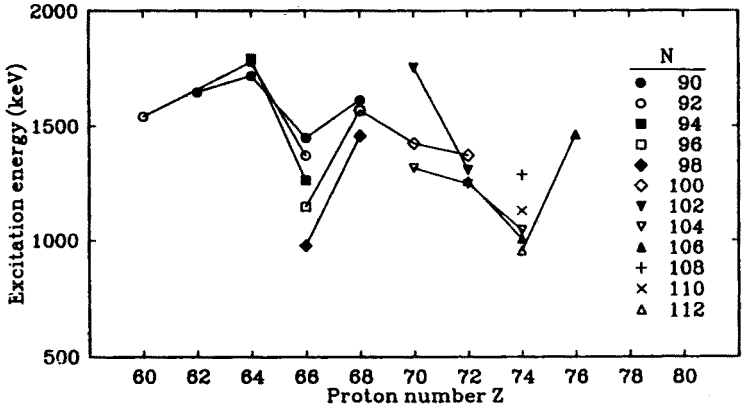


**Figure 11** Excitation energies of the $K^{\pi}=2^{-}$ bands in the A=150 region. For each isotonic chain the data have been connected by a solid line. (from Ref. [12]).

In the $K^{\pi}=1^{-}$ systematics (Fig. 10), one observes a sharp lowering along a narrow valley at neutron number N=94 associated with the two–quasineutron $\{\nu 5/2^{+}[642] - \nu 3/2^{-}[521]\}$ configuration [49]. The $K^{\pi}=1^{-}$ band in $^{156}$Sm, which we have tentatively identified [14] at the excitation energy of 803.5 keV, represents the lowest–lying $K^{\pi}=1^{-}$ band known in the rare–earth region [49]. However, as the minimum in the systematics of the $K^{\pi}=1^{-}$ bands has not been established, it is possible that the energy of this band is even lower in $^{154}$Nd. This could explain the sudden rise of the $K^{\pi}=0^{-}$ band in $^{152}$Nd (a trend that should also continue into $^{154}$Nd if the following logic is true). A sharp minimum can occur only if the occupation of a specific quasiparticle configuration is optimal. Consequently, the minima in the excitation energies for bands with different $K^{\pi}$ will be anticorrelated.

**Table 3** Energies of the $2_1^+$ states and deformation parameters $\beta_2$ of selected light lanthanides (from Ref. [11]).

| Nucleus | $E(2_1^+)$ [keV] | $\beta_2$ [a] | $\beta_2/\beta_{2(s.p.)}$ [a] |
|---|---|---|---|
| $^{150}$Nd | 130.1 | 0.285 | 10.75 |
| $^{152}$Sm | 121.8 | 0.306 | 11.91 |
| $^{154}$Gd | 123.1 | 0.310 | 12.49 |
| $^{156}$Dy | 137.9 | 0.293 | 12.16 |
| $^{152}$Nd | 72.6 | 0.333 | 12.5 |
| $^{160}$Gd | 75.3 | 0.353 | 14.22 |
| $^{164}$Dy | 73.4 | 0.348 | 14.45 |

[a] See Ref. [54] for a definition; data from Refs. [54,55].

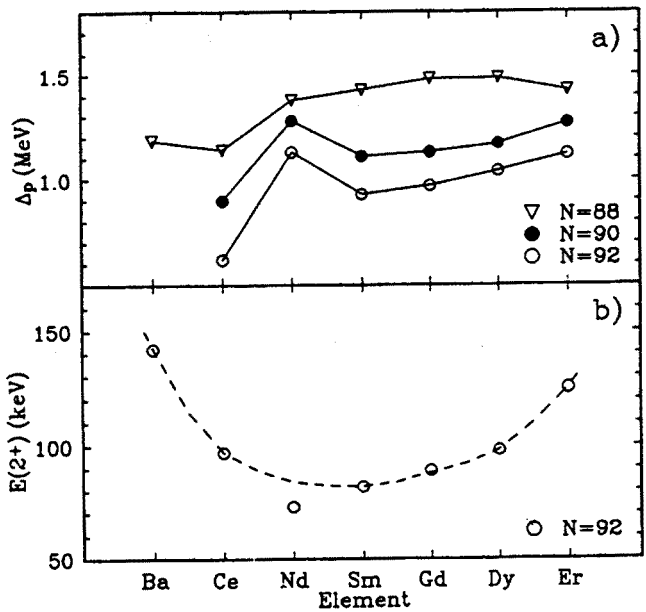


**Figure 12** (a) Proton pairing energies for a series of isotones. The deformed shell gap at Nd (Z=60) becomes significant for N=90,92. (b) Energies of the $2_1^+$ states for selected N=92 isotones. Its smooth trend is interrupted at $^{152}$Nd due to the increase in the moment of inertia of the g.s. band caused by the increase in the proton pairing gap. The dashed line serves only to guide the eye (from Ref. [11]).

To say it differently, lowering the $K^\pi=1^-$ band requires the $K^\pi=0^-$ band to rise in excitation energy since it is not likely to find optimal conditions for both excitations

in the same nucleus.

In the $K^\pi=2^-$ systematics of Fig. 11, the excitation energies show a sharp lowering along two narrow valleys at proton numbers Z=66 (dysprosium) and Z=74 (tungsten) associated with the two–quasiproton $\{\pi 7/2^-[523] - \pi 3/2^+[411]\}$ and $\{\pi 9/2^-[514] - \pi 5/2^+[402]\}$ configurations, respectively [49].

In summary, the systematics of the $K^\pi=1^-$ and $2^-$ bands show rather similar features that contrast with the pattern of the $K^\pi=0^-$ excitations. In both cases, one observes a sharp lowering of the excitation energies along well–defined neutron or proton numbers, indicating strong influence of the specific quasiparticle contributions. (In contrast, the lowering of the $K^\pi=0^-$ bands is along both neutron and proton numbers, giving a flat minimum.) However, as the minimum excitation energy is well below 1 MeV, it needs to be explained why the quasiparticle configurations should have such a profound influence on the excitation energies at energies as low as half the pairing energy gap.

### 4.2 Positive parity bands

$^{152}$Nd exibits the g.s. properties of a well–deformed nucleus (see Fig. 7), the energy of the $2_1^+$ state being among the lowest in the region. The corresponding large moment of inertia is, however, not simply a consequence of a large deformation as seen in Table 3. The g.s. of both $^{150}$Nd and $^{152}$Nd exhibit $\beta_2$ deformation parameters significantly lower than their neighboring nuclei, even in those cases where the moments of inertia of the Nd nuclei are higher. The deviation from the expected proportionality of the moment of inertia to the square of $\beta_2$ is remarkable. This effect, see Fig. 12, is likely due to a local variation of the strength of the (proton) pairing interaction, caused by the small deformed shell gap at Z=60 for deformation close to $\beta_2$=0.3.

The first three members of the first excited $K^\pi=0^+$ band (illustrated in Fig. 7) have been identified [11] in $^{152}$Nd. The rotational parameter $A$ of this band is about 50% larger than that of the g.s. band (Fig. 13), thus indicating different quadrupole deformation. A similar effect has been noticed in $^{150}$Nd [53]. As the lowest excited states of deformed nuclei can be viewed as predominantly composed of two–quasiparticle excitations, this effect must be a consequence of the excitation of valence nucleon pairs between orbitals with different deformation–driving properties [11]. This argument favours a shape–coexistence picture of the first excited $0^+$ bands in $^{150,152}$Nd. One should also note, that the $\gamma$ branchings from the first excited $K^\pi=0^+$ band to the g.s. band deviate strongly from the Alaga predictions for both $^{150}$Nd [53] and $^{152}$Nd [11].

## 5. $0_3^+$ Band in $^{152}$Sm

We have studied [13] levels in $^{152}$Sm as populated in the low–spin $\beta^-$ decay of $^{152}$Pm. A part of a revised decay scheme is illustrated in Fig. 14. As seen in Fig. 14, the $0_1^+$, $0_3^+$ (1082.7 keV), and $0_4^+$ (1658.4 keV) states are strongly $\beta$ fed

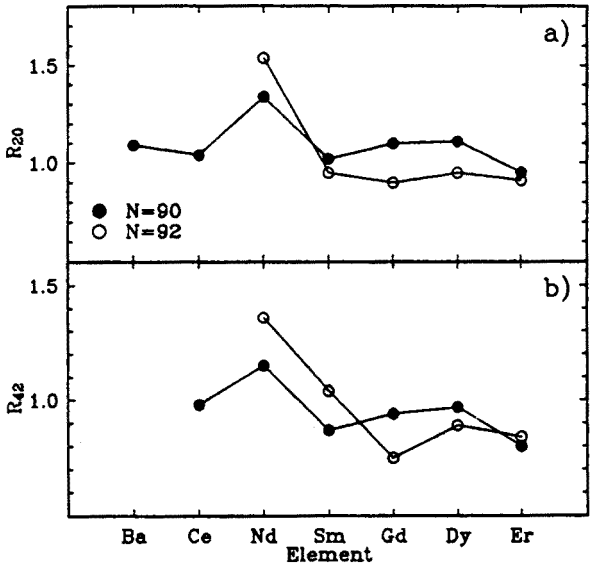


**Figure 13** (a) The ratio $R_{20} = \Delta E(2_\beta - 0_\beta)/\Delta E(2_g - 0_g)$ of the $2^+$–$0^+$ level spacings of the first excited $K^\pi=0^+$ and the g.s. bands of the N=90 and 92 isotones Ba–Er. (b) The corresponding ratio $R_{42} = \Delta E(4_\beta - 2_\beta)/\Delta E(4_g - 2_g)$. The low $R_{42}$ ratio obtained for $^{156}$Gd (N=92) may be due to a subshell effect at Z=64. (from Ref. [11]).

with log$ft$ ~6.5–7.1, while the feeding of the $0_2^+$ (684.8 keV) and $0_5^+$ (1736 keV, but not observed here) states is very weak (log$ft \leq$8.5). Half–lives of 15(6) ps and 8(5) ps were measured for the $0_3^+$ state at 1082.7 keV and for the $0_4^+$ state at 1658.4 keV, respectively, using a fast timing $\beta\gamma\gamma$(t) technique [3,4]. The newly measured transition rates for the $\beta'$ ($0_3^+$) band are compared in Table 4 to the pairing–plus–quadrupole (PPQ) calculations [15]. (The B(E2) rates for the $2_{\beta\prime}^+$ level were approximated from the relative intensities by adjusting the $\rho^2$(E0; $2_{\beta\prime}^+ \rightarrow 2_\beta^+$) rate to equal that of the $0_{\beta\prime}^+ \rightarrow 0_\beta^+$ transition.)

The microscopic PPQ calculations tested the hypothesis of shape–coexistence in $^{152}$Sm but yielded neither potential energy surfaces with two minima (one deformed and one spherical) nor an excited $0_3^+$ state with much smaller $\beta_{rms}$ than the g.s. These calculations were already found [15] in agreement with various experimental results for the lower–lying bands. However, it is their untested predictions for the $0_3^+$ band that represent the most controversial outcome of the Kumar calculations. As seen in Table 4, the agreement is very good for all nine B(E2) rates but poor for the two E0 transitions.

The new results confirm, for the first time, the interpretation of the $0_3^+$ band as the 'm' band (as defined by Kumar [15]) and also give weight to the controversial conclusion drawn by Kumar who questioned [15] the shape–coexistence interpreta-

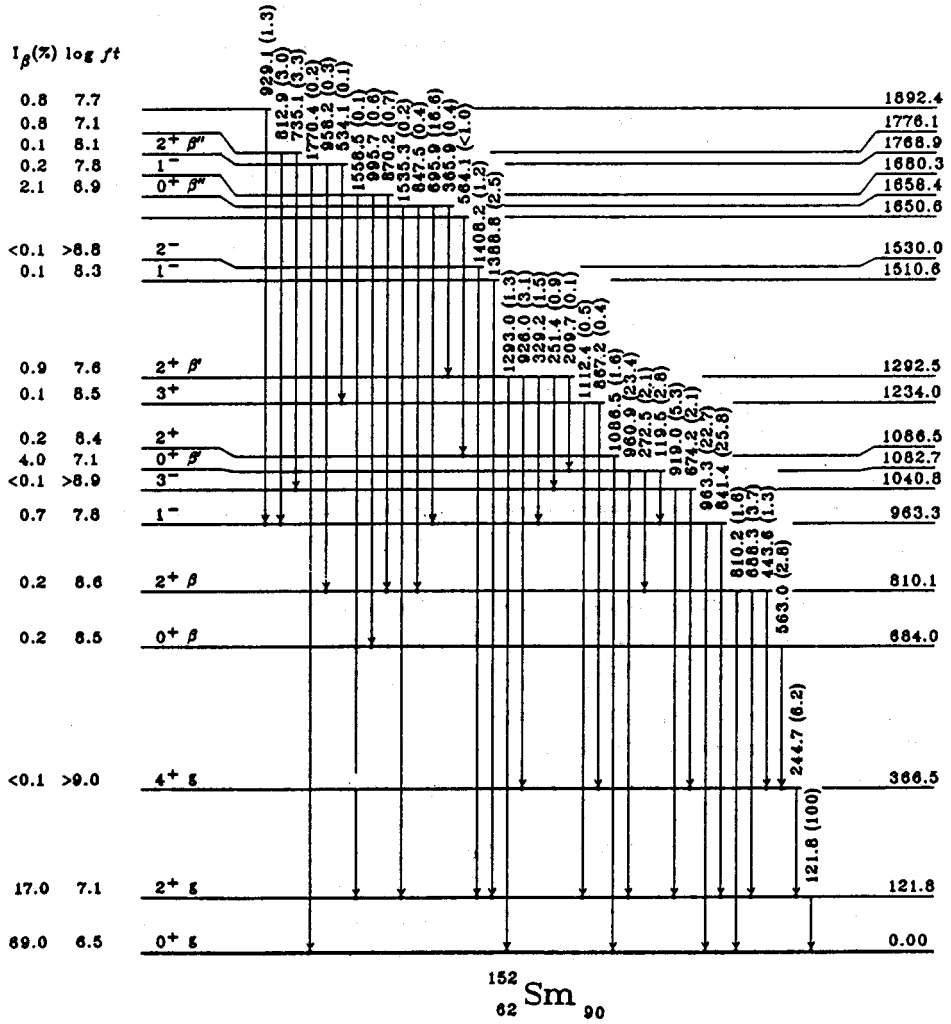


**Figure 14** A partial level scheme for the low–spin decay of $^{152}$Pm$\rightarrow^{152}$Sm. Labels '$g$', '$\beta$', '$\gamma$', '$\beta'$', and '$\beta''$' mark members of various bands discussed in the text (from Ref. [13]).

tion of the $0_3^+$ band and, as a consequence, of the Sm–Gd region. Further theoretical studies of the $\beta'$ bands are necessary but the real issue (raised by the new experimental data discussed in this Lecture) is whether the B(E2) and $\rho^2$(E0) rates and the $(p,t)$ and $(t,p)$ cross sections are in fact *shape independent* or not.

**Table 4** Transition rates deduced for the $\beta'$ ($0_3^+$) band in $^{152}$Sm (from Ref. [13]).

| $I_i \to I_f$ | B(E2) (W.u.) | PPQ [15] | $I_i \to I_f$ | $\rho^2$(E0) ($\times 10^3$) | PPQ [15] |
|---|---|---|---|---|---|
| $0_{\beta'} \to 2_g$ | 0.8(3) | 3.0 | $0_\beta \to 0_g$ | 83(9) | 133 |
| $2_{\beta'} \to 0_g$ | 0.21(11) [a] | 0.7 | $0_{\beta'} \to 0_g$ | 1.2(8) | 1.4 |
| $2_{\beta'} \to 2_g$ | 0.11(6) [a] | 0.07 | $0_{\beta'} \to 0_\beta$ | 21(9) | 195 |
| $2_{\beta'} \to 4_g$ | 2.7(14) [a] | 1.5 | $2_{\beta'} \to 2_\beta$ | $21^{Norm}$ | 153 |
| $0_{\beta'} \to 2_\beta$ | 40(16) | 82 | | | |
| $2_{\beta'} \to 0_\beta$ | $\leq$0.5 [a] | 0.34 | | | |
| $2_{\beta'} \to 2_\beta$ | 9(5) [a] | 8.4 | | | |
| $2_{\beta'} \to 4_\beta$ | 40(21) [a] | 34 | | | |
| $2_{\beta'} \to 0_{\beta'}$ | 184(100) [a] | 96 | | | |

[a] The uncertainty includes contribution due to normalization, see text.

## 6. Correspondence Interpretation of the Low–lying Bands in the Neutron–rich Sm and Gd Nuclei

The new results on $^{152}$Sm and the heavy Cd nuclei [34,38,39] challenge the shape–coexistence models or model interpretation of these regions of shape–coexistence. These results, however, are for different cases. The excited shape–coexistence structure is deformed in the vibrational $^{114}$Cd, while it is spherical in the deformed $^{152}$Sm. Furthermore, in $^{114}$Cd the shape–coexisting state is the first excited $0^+$ state, while in $^{152}$Sm it is the second one. The essence of findings on $^{114}$Cd [34] is that the B(E2) rates for the low–lying positive–parity levels (including the intruder band) fit best a pattern predicted for quadrupole vibrational multiplets. Such case could be similar to the lighter Sm nuclei, which are vibrational, and then one could follow the evolution of the vibrational multiplets (which would include the intruder states) towards the deformed bands across a shape transition at N=88/90.

As the first step of the analysis we note, that the high selectivity of the $\beta^-$ decay is also seen in the $(p,t)$ reactions (and perhaps in the $(t,p)$ as well). The $0_3^+$ and $0_4^+$ ($0_2^+$ and $0_5^+$) states in heavy Sm/Gd nuclei are strongly (barely) populated in the $(p,t)$ reaction [56], while the $(t,p)$ reaction [57] populates the $0_3^+$ state with an exceptional strength. This selectivity provides a natural classification of the first and second excited $0^+$ states in the transitional Sm and Gd nuclei (at N=86–96). (The Gd data supplements the Sm systematics.) The $\beta$ sequence is strongly populated in the $(p,t)$ reaction and weakly in the $(t,p)$ transfer while the $\beta'$ sequence shows the opposite features. The excitation energies for the $\beta'$ sequence remain almost constant (see Fig. 15), while those for the $\beta$ sequence change widely. This shows again that the $\beta$ and $\beta'$ sequences have different intrinsic structures.

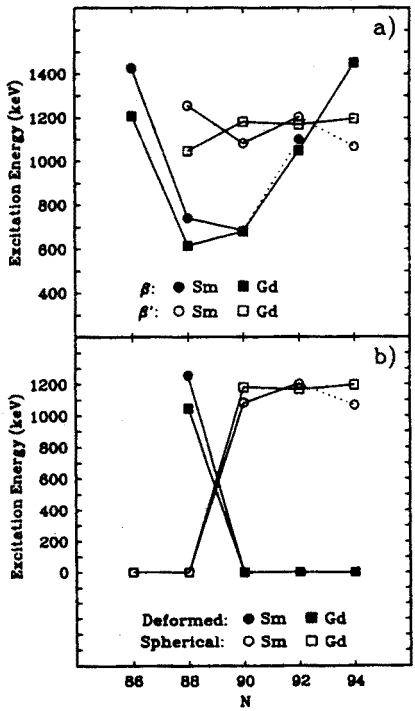


**Figure 15** (a) Excitation energies of the $\beta$ and $\beta'$ sequences of $0^+$ states in heavy Sm and Gd. (b) Same as (a) but for the 'deformed' and 'spherical' sequences. The 'spherical' sequence includes the g.s. bands for N≤88 and the $\beta'$ ($0_3^+$) bands for N≥90, while the 'deformed' sequence includes the $\beta'$ ($0_3^+$) band for N=88 and the g.s. bands for N≥90 (from Ref. [13]).

The relative level energies within the g.s., $\beta$, and $\beta'$ band sequences evolve smoothly from vibrational towards rotational patterns — all showing similar behaviour (see Fig. 16). If one breaks the g.s. and $\beta'$ sequences into the shape–coexisting 'deformed' and 'spherical' sequences (Figs. 15 and 17), then again the 'deformed' ('spherical') sequence shows a smooth decrease of the relative $2^+$, $4^+$, and $6^+$ energies and the increase of the energy ratios $R(4^+/2^+)$ from moderately deformed (vibrational) at N=88 to fully deformed at N=96. (R= ~2.8, 3.01, 3.25, 3.29 for $^{150-156}$Sm and 2.39, 3.01, 3.24, 3.29 for $^{152-158}$Gd for the 'deformed' and 2.15, 2.31, 2.52, 3.23 for $^{148-154}$Sm, and 2.02, 2.19, 2.19, 3.27, 3.30 for $^{150-158}$Gd for the 'spherical' sequences.) These results disagree with the 'shape–coexistence' interpretation which presupposes either stable spherical and deformed shapes or clearly defined shape differences. Only at N=84–90 does the 'spherical' band sequence appear to be significantly less deformed than the 'deformed' one (see Fig. 17).

The $^{152}$Sm and $^{114}$Cd results follow the correspondence interpretation [16,17] (here extended to include the pattern of B(E2) rates) which provides a schematic

**Figure 16** (below left) Relative excitation energies within the g.s., $\beta$ and $\beta'$ sequences of bands in heavy Sm (solid circles connected by solid lines) and Gd (open circles connected by broken lines). Note discontinuities at N=88/90 for the $\beta$ and $\beta'$ bands (from Ref. [13]).

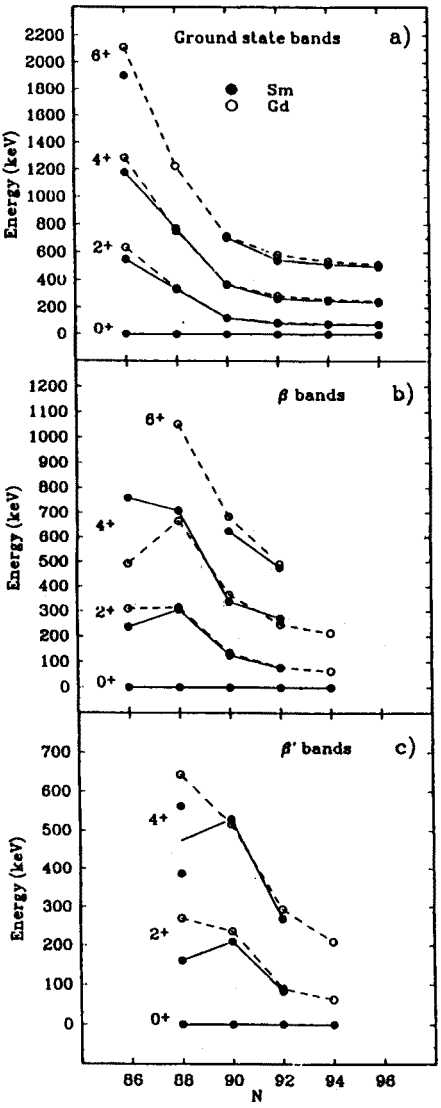


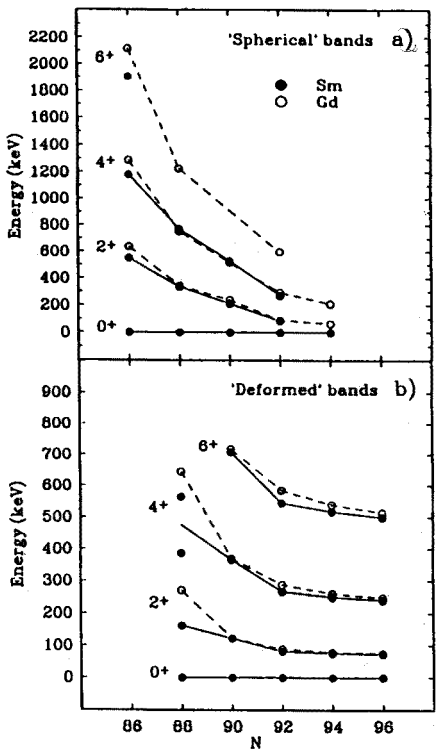


**Figure 17** (above right) Relative excitation energies within the 'deformed' and 'spherical' sequences of bands in heavy Sm (solid circles connected by solid lines) and Gd (open circles connected by broken lines) (from Ref. [13]).

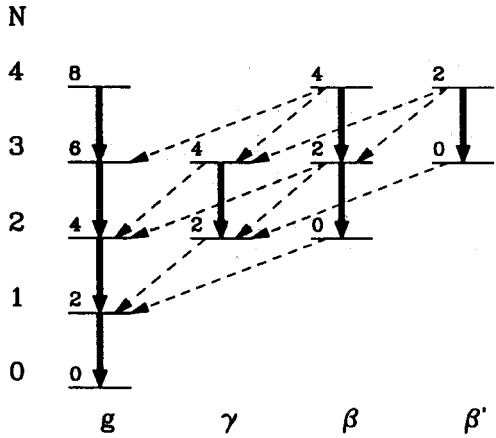


**Figure 18** The 'correspondence' relation [16,17] between the quadrupole vibrational multiplets and the g.s., $\beta$, $\gamma$ and $\beta'$ bands in the rotational nuclei. Only selected levels are indicated, marked by the level spin (above the level bar) and by the phonon number N (in the leftmost column). Fast vibrational $\Delta N=1$ transitions which evolve towards fast intraband (slow interband) rotational transitions are marked by solid (broken) arrows. Their B(E2) pattern is 'fast' ('transitional'). Other transitions (not shown) are forbidden in the vibrational limit ($\Delta N \geq 2$) and evolve towards slow interband transitions. Their B(E2) pattern is 'slow' (from Ref. [13]).

representation of the smooth structural changes that occur in the transition from vibrational to rotational nuclei and gives a bench–mark to classify the experimental data and to uncover major departures from its simple patterns. In particular, levels of the quadrupole vibrational multiplets (spherical nuclei) evolve into the levels of the g.s., $\beta$, $\gamma$, and $\beta'$ bands in the deformed nuclei [16,17] as schematically shown in Fig. 18. Importantly, we make here no distinction for the intruder states. Moreover, each B(E2) rate should follow one of the three patterns that is predetermined by the position of the transition in the vibrational scheme of Fig. 18. Three distinctive B(E2) patterns are expected [13]: 'fast' (consistently high rates at ~50–100 W.u.), 'slow' (consistently low rates at $\geq$1 W.u.), and 'transitional' — a smooth decrease of transition rates by ~2 orders of magnitude from ~ 100 W.u. to ~1 W.u.

The $\beta$ and $\beta'$ sequences defined above overlap with those of the correspondence interpretation, provided (which is critical here) that the shape–coexisting $\beta'$ bands can be treated as part of these dynamically evolving phonon multiplets. Out of 17 individual B(E2) rates obtained for transitional Sm and Gd, 13 in Sm and 14 in Gd follow the predetermined patterns, while 4 in Sm and 3 in Gd do not. (Data for Sm and Gd, which are almost identical, are summarized in Figs. 19 and 20 and Table 5; for a detailed discussion see Ref. [13].) Thus, 80% of the B(E2) rates for the $\beta$, $\gamma$, and $\beta'$ bands follow the correspondence patterns. The remaining

**Figure 19** (below left) B(E2) systematics for the intraband $\beta \rightarrow \beta$ and interband $\beta \rightarrow$ g.s. transitions in heavy Sm and Gd. Note, the expected 'transitional' ($0^+_\beta \rightarrow 2^+_g$ and $2^+_\beta \rightarrow 4^+_g$), 'fast' ($2^+_\beta \rightarrow 0^+_\beta$), and 'slow' ($2^+_\beta \rightarrow 0^+_g$) patterns. The exception is the $2^+_\beta \rightarrow 2^+_g$ pattern predicted to be 'slow', but where the B(E2) rates vary from low values (~1 W.u.) in both limits to rather high values (~17–68 W.u.) in the transitional region in between (from Ref. [13]).

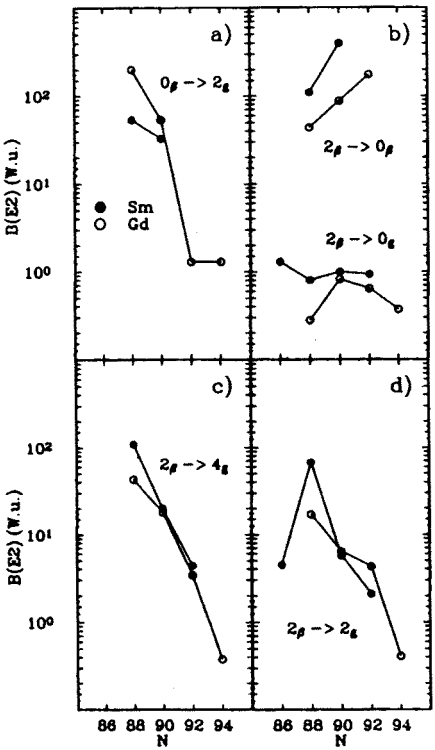


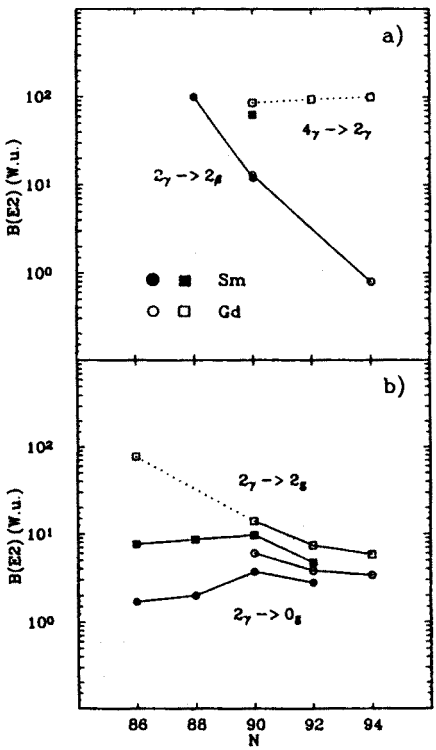


**Figure 20** (above right) **(a):** B(E2) systematics for the intraband $4_\gamma \rightarrow 2_\gamma$ (squares) and interband $2_\gamma \rightarrow 2_\beta$ (circles) transitions in heavy Sm and Gd. **(b):** Same as (a) but for the $2_\gamma \rightarrow 0_g$ (circles) and $2_\gamma \rightarrow 2_g$ (squares) transitions (from Ref. [13]). Note, the expected 'fast' ($4^+_\gamma \rightarrow 2^+_\gamma$) and 'transitional' ($2^+_\gamma \rightarrow 2^+_\beta$) patterns. The overall pattern for the $2^+_\gamma \rightarrow 0^+_g$ transition is 'slow', as expected, but at higher B(E2) rates of ~3 W.u. The $2^+_\gamma \rightarrow 2^+_g$ pattern (expected to be 'transitional') is approximately followed in Gd, while in Sm the pattern is rather flat with B(E2) rates of ~8 W.u. (at N=86–88), which is lower than the expected rates of ~40–100 W.u. The lower rates in this case could be correlated and somewhat complementary to the higher rates observed in Fig. 19 for the $2^+_\beta \rightarrow 2^+_g$ pattern.

**Table 5** Systematics of the experimental B(E2) and $\rho^2$(E0) rates from the $\beta'$ band in heavy Sm and Gd (from Ref. [13]).††

| $I_i \to I_f$ | $^{150}Sm_{88}$ | $^{152}Sm_{90}$ | $^{152}Gd_{88}$ | $^{154}Gd_{90}$ | $^{156}Gd_{92}$ | $^{158}Gd_{94}$ |
|---|---|---|---|---|---|---|
| | | | B(E2) [W.u.] | | | |
| $0_{\beta'} \to 2_g$ | 0.17 | 0.8(3) | 1.4 | | 3.4(10) | |
| $2_{\beta'} \to 0_g$ | 0.00004 | 0.21(11) | 0.033 | 0.035 | 0.31(2) | 0.31(4) |
| $2_{\beta'} \to 2_g$ | 0.19 | 0.11(6) | 1.3 | 0.065 | 1.2(1) | 0.24 |
| $2_{\beta'} \to 4_g$ | <1.6 | 2.7(14) | 0.41 | 1.1 | 4.3(4) | 1.4(2) |
| $0_{\beta'} \to 2_\beta$ | 29 | 40(16) | | | | |
| $2_{\beta'} \to 0_\beta$ | <1.2 | ≤0.5 | 1.6 | <1 | <0.3 | |
| $2_{\beta'} \to 2_\beta$ | 11 | 9(5) | 16. | 11. | | |
| $2_{\beta'} \to 4_\beta$ | | 40(21) | | 21. | | |
| $2_{\beta'} \to 2_\gamma$ | 13 | | 21. | <2 | 19(6) | |
| $2_{\beta'} \to 0_{\beta'}$ | [110][a] | 184(100) | [100][a] | [200][a] | | |
| | | | $\rho^2$ [×10$^3$] | | | |
| $0_{\beta'} \to 0_g$ | 1.2 | 1.2(8) | 3.9 | | 3.0(13) | |
| $2_{\beta'} \to 2_g$ | 1.6 | | 3.4 | >0.8 | | 0.6(2) |
| $0_{\beta'} \to 0_\beta$ | [42][a] | 21(9) | [153][a] | | 32(15) | |
| $2_{\beta'} \to 2_\beta$ | 42 | [21][a] | 153. | 67 | | |
| $2_{\beta'} \to 2_\gamma$ | 17 | | | | | |

[a] For $^{150}$Sm and $^{152,154}$Gd the absolute rates were approximated: first for the $2^+_{\beta'}$ state by setting the fast intraband B(E2; $2^+_{\beta'} \to 0^+_{\beta'}$) rate equal to 110, 100, and 200 W.u., respectively, and then for the $0^+_{\beta'}$ state by setting the $\rho^2$(E0; $0^+_{\beta'} \to 0^+_\beta$) and $\rho^2$(E0; $2^+_{\beta'} \to 2^+_\beta$) rates equal. Uncertainties (expected to be large) are not provided for the approximated results.

†† Six B(E2) patterns follow the expectations: one 'fast' ($2^+_{\beta'} \to 0^+_{\beta'}$) and five 'slow' ($0^+_{\beta'} \to 2^+_g$, $2^+_{\beta'} \to 0^+_g$, $2^+_{\beta'} \to 2^+_g$, $2^+_{\beta'} \to 4^+_g$, and $2^+_{\beta'} \to 0^+_\beta$). Two sequences involving the $2^+_\beta$ and $2^+_\gamma$ states somewhat deviate from the expected patterns. By now this deviation is fully expected, and in fact, necessary if the data are to be self-consistent. The apparent 'mixing effect' of the $2^+_\gamma$ and $2^+_\beta$ states is to lower the fast 'transitional' and 'fast' rates and to raise the 'slow' rates. It is seen for the $2^+_{\beta'} \to 2^+_\beta$ transition. Our data for N=88 and 90 show B(E2) rates at 9–16 W.u., lower than the expected 'transitional' rate of 40–100 W.u. Similarly, significantly higher values of 13–21 W.u. are observed for the $2^+_{\beta'} \to 2^+_\gamma$ transition predicted to be 'slow' at ∼1 W.u.

discrepancies can be traced to the 'mixing effect' of the $2^+_\beta$ and $2^+_\gamma$ states in the transitional region, where the high 'transitional' and 'fast' rates are lowered while the 'slow' rates are increased.

We interpret the results for $^{114}$Cd and $^{152}$Sm as supporting the correspondence relations [16,17] between levels of the quadrupole vibrational multiplets in the spherical nuclei and the g.s., $\beta$, and $\gamma$ bands in the deformed nuclei extended to include the $0^+_3$ states as suggested by Sakai [17].

The $\beta$ and $\gamma$ bands which band–heads evolve from the N=2 vibrational multiplets represent two basic excitation modes. One may ask whether the $\beta'$ band, which band–head evolves from the N=3 multiplet, is also associated with a distinctively different excitation mode as well. A number of facts, such as the uncorrelated excitation energies for the $\beta$ and $\beta'$ bands in heavy Sm and Gd (Fig. 15), the high selectivity of the $\beta^-$ decay (Fig. 14), and the closely anticorrelated high selectivity of the $(p,t)$ reaction for $^{152}$Sm, affirm that the $\beta$ and $\beta'$ states have different intrinsic structures. Yet the $\beta$, $\gamma$, and $\beta'$ bands show also common features like smooth correlations of the relative excitation energies and of the transition rates. Thus the $\beta'$ band could represent a new mode of intrinsic excitation in par with the $\beta$ and $\gamma$ modes. Yet $\beta'$, as the N=3 mode of excitation, could be more complex than the N=2 $\beta$ and $\gamma$ modes. This could explain the inability of the phenomenological models based on a severely truncated space (like IBA) to account for the band and the neccessity to invoke the intruder picture.

## 7. 'Di–nature' of the excited $0^+$ bands

Properties of the low–lying $0^+$ states remain puzzling. Their population (through reaction or $\beta$ decay) and deexcitation processes frequently reveal equally strong evidence for different (apparently inconsistent) components in the wave functions [39,49]. The shape–coexisting Cd and Sm/Gd nuclei discussed in Sections 2 and 6 could illustrate this point. Although some evidence [8,25,35] points towards existence of low–lying intruder structures with vastly different shapes, a number of properties can be explained without invoking shape–coexistence [15] or in fact negating various aspects of the current shape–coexistence models [34,39]. In the case of the two close–lying $0^+$ states in $^{114}$Cd there is even a confusion which one of them is the shape–coexisting intruder as the expected properties seem to alternate between the levels but in a way that would negate strong configuration mixing [34,39]. Despite these complications the B(E2) transition rates within and in between the bands generally follow [13,34] simple 'correspondence' patterns.

In general one would expect the g.s. and excited bands to have similar moments of inertia and/or deformation. A band that departs from this expectation is considered anomalous or intruder. The essence of the shape–coexisting models [25,35] is that the intruder band, which shows a moment of inertia strongly different from the g.s. structure, is associated with its own minimum in a potential well. Transitions from this band to the g.s. structure are forbidden or strongly retarded

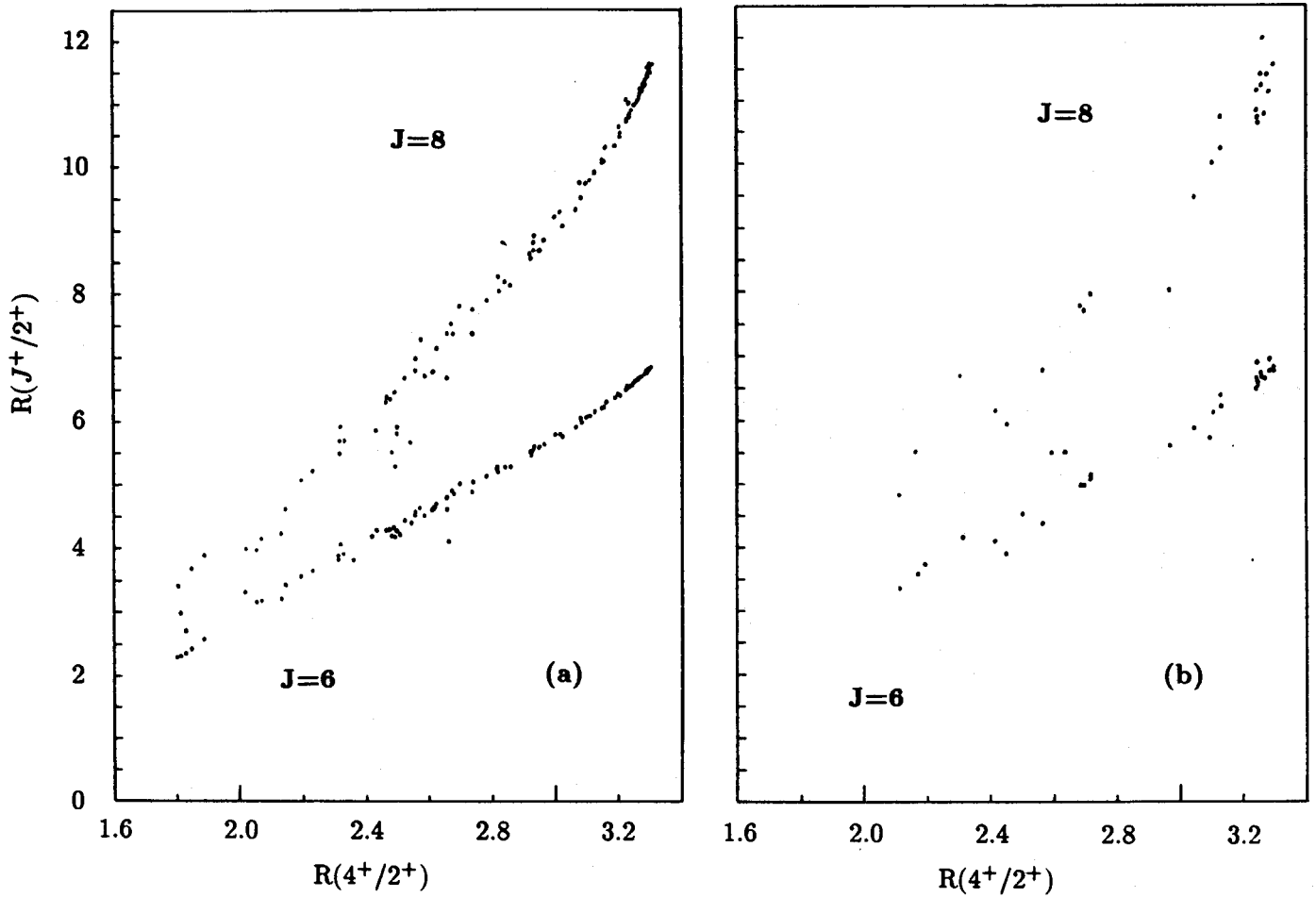


Figure 21

unless there is a configuration mixing. However, as discussed in section 2, a strong configuration mixing is required that can invert the decay properties of the $0_2^+$ and $0_3^+$ states like for $^{116}$Sn or $^{114}$Cd [25,35].

One may ask, however, whether this mixing and inversion of transition rates is in fact necessary? In this section (based on Ref. [18]) we want to explore an alternative proposition — of 'di–nature' of the low–lying collective bands (which is not necessarily limited to the $0^+$ bands). Namely, that the excited $0^+$ bands show a duality of conflicting properties as a general feature, not acquired through strong mixing. These bands, which show individual properties (like moments of inertia, high selectivity in the particle transfer reactions or $\beta$ decay) based on different intrinsic (quasiparticle) structures, and follow at the same time also a common pattern of intra– and interband transition rates predicted by simple models (like the quadrupole vibrational model for $^{114}$Cd [34]). Di–nature clearly emphasizes the importance of dynamical effects in nuclei.

In the present discussion we consider all excited $0^+$ bands to be dominated by individual intrinsic excitations even for nuclei that are not deformed. The intruder states thus loose their special status. Furthermore, since strong mixing is no longer necessary, any excited $0^+$ band would appear as a 'second g.s. structure'.

Fig. 21(a) illustrates the Mallmann plot [58] for the g.s. bands in the A=150–190 region while Fig. 21(b) illustrates the same plot for all known excited $0^+$ bands for A>56 (data from Refs. [17,49]). The relative energy ratios $8^+/2^+$ and $6^+/2^+$ for the excited $0^+$ bands plotted against the $4^+/2^+$ ratio not only form its own pattern (thus indicating weak mixing with other levels), but in fact follow exactly the same patterns as the g.s. bands. This latter feature confirms that the excited $0^+$ bands show a general property of a (second) g.s. Note, that due to the experimental difficulties the data on the excited bands are not only scarce but also less reliable than those for the g.s. bands.

In the next step we examine the relationship between the deformation of the g.s. and that for the excited $0^+$ bands. Fig. 22(a) illustrates the ratio of the relative energies of the $2^+$ states for the excited band (labelled '$\sigma$') and the g.s. band plotted against One could have expected á priori that the data points (excluding a few intruder states) would follow a horizontal line at the E/E ratio of 1. Instead the data are generously scattered. For a detailed discussion of Fig. 22 the reader is referred to Ref. [18], we only note that the $2^+$ energies of the excited states are significantly lower than those for the g.s. structures in two regions: for the magic/spherical nuclei (R<2.4) and for the strongly deformed ones (R$\sim$3.3).

Fig. 22(b) illustrates the ratio of the $4^+/2^+$ ratios for the excited and the g.s. bands plotted agains the $4^+/2^+$ ratio for the g.s. band. Although one observes a scatter of points, they are not so widely dispersed as those in Fig. 22(a). We will not discuss this Figure in detail, except to mention that it is consistent with the systematics of Fig. 22(a). Note, if the scatter of points in these Figures would be due to the configuration mixing then neither the g.s. nor the excited bands would

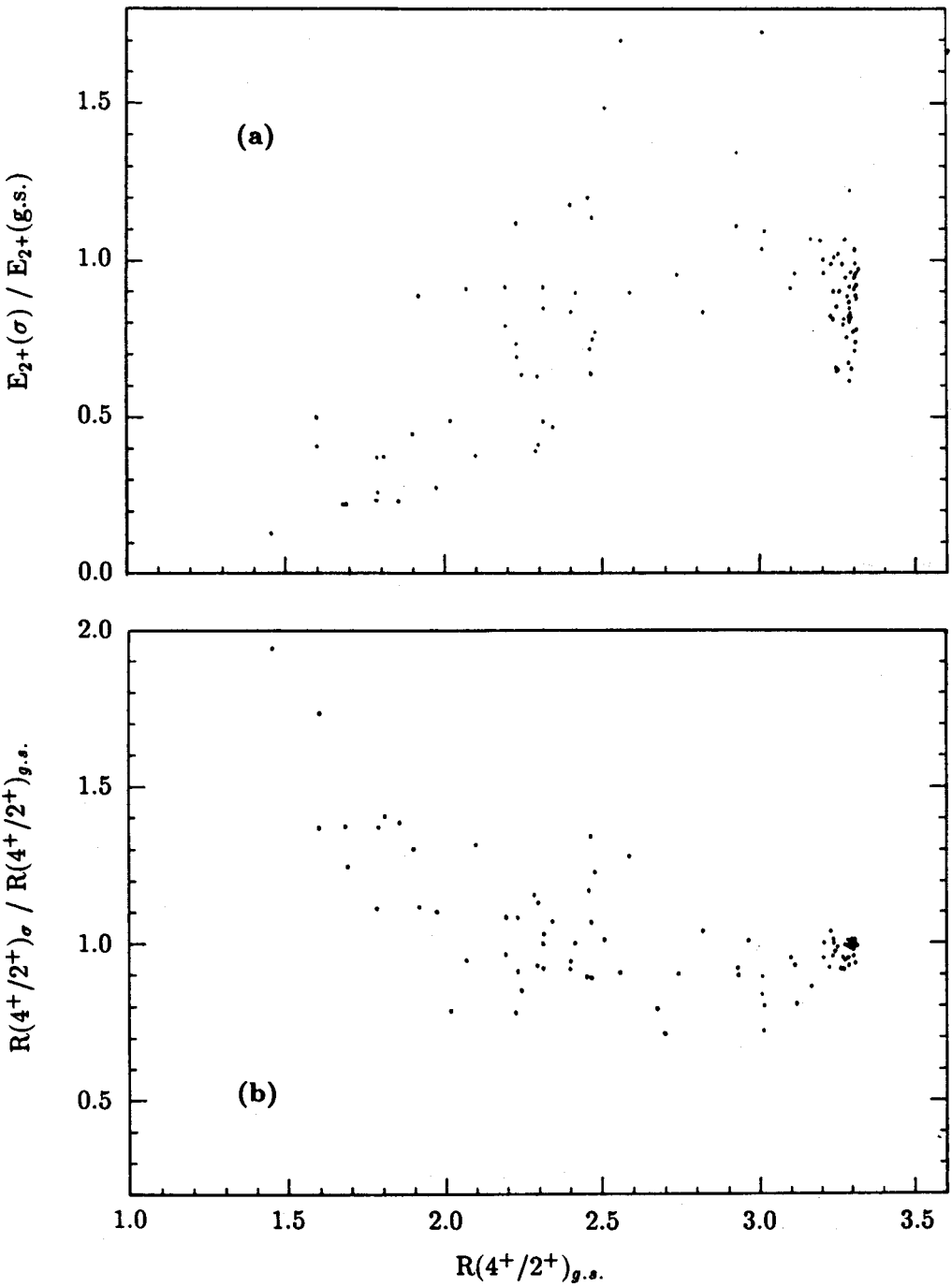


**Figure 22**

follow the Mallmann plots (Fig. 21) so well. There are also other arguments against strong mixing already raised in the previous sections. Thus one may conclude that in general the moments of inertia and/or deformation of the g.s. and excited bands are different. Consequently, it is an exception, rather than a rule, for these parameters to be the same for different bands in a given nucleus.

The issue of 'di–nature' of the excited bands should be further explored. There is a strong need for a more complete and reliable systematics of the excited bands and particularly of the absolute transition rates. One should also reexamine the nature of strong E0 rates in the absence of strong configuration mixing of shape–coexisting states.

## Summary

A new generation of experiments carried out at OSIRIS takes advantage of the high beam intensities from an improved ISOL–facility and a higher detection sensitivity from multidetector arrangements. Furthermore, these experiments include fast timing $\beta\gamma\gamma(t)$ measurements which unravel crucial lifetime information.

The new experiments bring important data on the regions/issues of special interest: structure of doubly–magic $^{132}$Sn and the nature of the excited $0^+$ and the low–lying octupole bands in the medium heavy nuclei.

## References

1. L. Jacobsson, B. Fogelberg, B. Ekström, and G. Rudstam, Nucl. Instr. Meth. Phys. Res. **B26**, 223 (1986).
2. B. Fogelberg, M. Hellström, L. Jacobsson, D. Jerrestam, L. Spanier, and G. Rudstam, Nucl. Instr. Meth. Phys. Res. **B**, in press.
3. H. Mach, R.L. Gill and M. Moszyński, Nucl. Instr. Meth. **A280**, 49 (1989).
4. M. Moszyński and H. Mach, Nucl. Instr. Meth. **A277**, 407 (1989).
5. M. J. Martin, Nucl. Data Sheets **47**, 797 (1986), and references therein.
6. Yu. V. Sergeenkov, Nucl. Data Sheets **65**, 277 (1992), and references therein.
7. B. Fogelberg, M. Hellström, D. Jerrestam, A. Kerek, H. Mach, L.O. Norlin, J.P. Omtvedt, and H. Prade, *6th International Conference on Nuclei far from Stability and 9th International Conference on Atomic Masses and Fundamental Constants*, Bernkastel–Kues, Germany, July 19–24, 1992, in press.
8. A. Passoja, J. Kantele, M. Luontama, R. Julin, E. Hammaren, P.O. Lipas, and P. Toivonen, J. Phys. **G12**, 1047 (1986), and references therein.
9. P. Kleinheiz, Physica Scripta **24**, 236 (1981).
10. H. Mach, W. Nazarewicz, D. Kusnezov, M. Moszyński, B. Fogelberg, M. Hellström, L. Spanier, R.L. Gill, R.F. Casten, and A. Wolf, Phys. Rev. **C41** R2469 (1990), and references therein.
11. M. Hellström, B. Fogelberg, H. Mach, D. Jerrestam, and L. Spanier, Phys.

Rev. C, in press.
12. M. Hellström, H. Mach, B. Fogelberg, D. Jerrestam, and L. Spanier, Phys. Rev. C, submitted.
13. H. Mach, M. Hellström, B. Fogelberg, D. Jerrestam, and L. Spanier, Phys. Rev. C, submitted.
14. M. Hellström, B. Fogelberg, L. Spanier, and H. Mach, Phys. Rev. **C41**, 2325 (1990).
15. K. Kumar, Nucl. Phys. **A231**, 189 (1974), and references therein.
16. R.K. Sheline, Rev. Mod. Phys. **32**, 1 (1960).
17. M. Sakai, Nucl. Phys. **A104**, 301 (1967), also At. Data Nucl. Data Tables **31**, 399 (1984).
18. H. Mach and B. Fogelberg, to be published.
19. H. Mach, *Proceedings of XXV Zakopane School on Physics*, edited by J. Styczeń and Zb. Stachura (World Scientific, Singapore, 1990) Vol. 2, p. 77, and references therein.
20. H. Ohm, G. Lhersonneau, K. Sistemich, B. Pfeiffer, and K.-L. Kratz, Z. Phys. **A327**, 483 (1987).
21. H. Mach, M. Moszyński, R.L. Gill, F.K. Wohn, J.A. Winger, John C. Hill, G. Molnár, and K. Sistemich, Phys. Lett. **B230**, 21 (1989).
22. H. Mach, F.K. Wohn, G. Molnár, K. Sistemich, John C. Hill, M. Moszyński, R.L. Gill, W. Krips, and D.S. Brenner, Nucl. Phys. **A523**, 197 (1991), and references therein.
23. P. Federman and S. Pittel, Phys. Rev. **C20**, 820 (1979).
24. A. Etchegoyen, P. Federman, and E.G. Vergini, Phys. Rev. **C39**, 1130 (1989).
25. G. Wenes, P. Van Isacker, M. Waroquier, K. Heyde, and J. Van Maldeghem, Phys. Rev. **C23**, 2291 (1981).
26. K. Heyde and R.A. Meyer, Phys. Rev. **C37**, 2170 (1988), also Phys. Rev. **C42**, 790 (1990).
27. H. Mach, G. Molnár, S.W. Yates, R.L. Gill, A. Aprahamian, and R.A. Meyer, Phys. Rev. **C37**, 254 (1988).
28. H. Mach, M. Moszyński, R.L. Gill, G. Molnár, F.K. Wohn, J.A. Winger, and John C. Hill, Phys. Rev. **C41**, 350 (1990), also Phys. Rev. **C42**, 793 (1990).
29. K. Kawade, G. Battistuzzi, H. Lawin, H.A. Selić, K. Sistemich, F. Schussler, E. Monnand, J.A. Pinston, B. Pfeiffer, and G. Jung, Z. Phys. **A304**, 293 (1982).
30. G. Lhersonneau, H. Gabelmann, B. Pfeiffer, K.-L. Kratz, the OSTIS, ISOLDE and IGISOL Collaborations, *6th International Conference on Nuclei far from Stability and 9th International Conference on Atomic Masses and Fundamental Constants*, Bernkastel-Kues, Germany, July 19–24, 1992, in press.
31. R.A. Meyer, E.A. Henry, L.G. Mann, and K. Heyde, Phys. Lett. **177B**, 271 (1986).

32. M.L. Stolzenwald, S. Brant, H. Ohm, K.Sistemich, and G. Lhersonneau, *Nuclear Structure of the Zirconium Region*, edited by J. Eberth, R.A. Meyer and K. Sistemich, (Springer-Verlag, Berlin, 1988), p. 239.
33. H. Mach, G. Molnár, K. Sistemich, B. Fogelberg, M. Hellström, L. Spanier, M. Moszyński, J. Winger, R.L. Gill and B. Mach, to be published.
34. C. Fahlander, A. Bäcklin, L. Hasselgren, A. Kavka, V. Mittal, L.E. Svensson, B. Varnestig, D. Cline, B. Kotliński, H. Grein, E. Grosse, R. Kulessa, C. Michel, W. Spreng, H.J. Wollersheim, and J. Stachel, Nucl. Phys. **A485**, 327 (1988).
35. K. Heyde, P. Van Isacker, M. Waroquier, G. Wenes, and M. Sambataro, Phys. Rev. **C25**, 3160 (1982).
36. A. Aprahamian, D.S. Brenner, R.F. Casten, R.L. Gill, A. Piotrowski, and K. Heyde, Phys. Lett. **140B**, 22 (1984).
37. A. Aprahamian, Ph.D. Thesis, Clark University, (1985) p. 189.
38. H. Mach, M. Moszyński, R.F. Casten, R.L. Gill, D.S. Brenner, J.A. Winger, W. Krips, C. Wesslborg, M. Büscher, F.K. Wohn, A. Aprahamian, D. Alburger, A. Gelberg, and A. Piotrowski, Phys. Rev. Lett. **63**, 143 (1989).
39. J. Kumpulainen, R. Julin, J. Kantele, A. Passoja, W.H. Trzaska, E. Verho, and J. Väärämäki, Z. Phys. **A335**, 109 (1990), also Phys. Rev. **C45**, 640 (1992).
40. G. Molnár, T. Belgya, B. Fazekas, A. Veres, S.W. Yates, E.W. Kleppinger, R.A. Gatenby, R. Julin, J. Kumpulainen, A. Passoja, and E. Verho, Nucl. Phys. **A500**, 43 (1989).
41. H. Mach, E.K. Warburton, R.L. Gill, R.F. Casten, J.A. Becker, B.A. Brown, and J.A. Winger, Phys. Rev. **C41**, 226 (1990).
42. H. Ohm, M. Liang, G. Molnár, S. Raman, K. Sistemich, and W. Unkelbach, Phys. Lett. **B241**, 472 (1990).
43. H. Mach, S. Ćwiok, W. Nazarewicz, B. Fogelberg, M. Moszyński, J. Winger, and R.L. Gill, Phys. Rev. **42**, R811 (1990).
44. F. Buchinger, E.B. Ramsay, E. Arnold, W. Neu, R. Neugart, K. Wendt, R.E. Silverans, P. Lievens, L. Vermeeren, D. Berdichevsky, R. Fleming, D.W.L. Sprung, and G. Ulm, Phys. Rev. **C41**, 2883 (1990).
45. T. Björnstad, M.J.G. Borge, J. Blomqvist, R.D. von Dincklage, G.T. Evan, P. Hoff, B. Jonson, K. Kawade, A. Kerek, O. Klepper, G. Lövhöiden, S. Mattsson, G. Nyman, H.L. Ravn, G. Rudstam, K. Sistemich, O. Tengblad, and the ISOLDE Collaboration, Nucl. Phys. **A453**, 463 (1986).
46. K. Kawade, K. Sistemich, G. Bathistuzzi, H. Lawin, K. Shizuma, and J. Blomqvist, Z. Phys **A308**, 33 (1982).
47. B. Fogelberg and J. Blomqvist, Nucl. Phys. **A429**, 205 (1984).
48. S. Rohoziński, Rep. Prog. Phys. **51**, 541 (1988), and references therein.
49. P. C. Sood, D. M. Headly, and R. K. Sheline, At. Data Nucl. Data Tables **47**, 89 (1991).

50. T. Karlewski, N. Hildebrand, M. Brugger, N. Kaffrell, N. Trautmann, and G. Herrmann, Z. Phys **A330**, 55 (1988).
51. H. Mach, A. Piotrowski, R.L. Gill, R.F. Casten, and D.D. Warner, Phys. Rev. Lett. **56**, 1547 (1986).
52. M. Hellström, B. Fogelberg, H. Mach, D. Jerrestam, and L. Spanier, *6th International Conference on Nuclei far from Stability and 9th International Conference on Atomic Masses and Fundamental Constants*, Bernkastel–Kues, Germany, July 19–24, 1992, in press.
53. B. Fogelberg and G. Skarnemark, Nucl. Phys. **A453**, 15 (1986).
54. S. Raman, C.H. Malarkey, W.T. Milner, C.W. Nestor, Jr., and P.H. Stelson, At. Data Nucl. Data Tables **36**, 1 (1987).
55. M. Hellström, H. Mach, B. Fogelberg, D. Jerrestam, and L. Spanier, Phys. Rev. **C43**, 1462 (1991).
56. A. Saha, O. Scholten, D.C.J.M. Hageman, and H.T. Fortune, Phys. Lett. **B85**, 215 (1979), and references therein.
57. S. Hinds, J.H. Bjerregaard, O. Hansen, and O. Nathan, Phys. Lett. **14**, 48 (1965).
58. C.A. Mallmann, Phys. Rev. Lett. **2**, 507 (1959).